PHYSICAL REVIEW B **72**, 020103(R) (2005)

Transition from the Rh_2O_3(II)-to-$CaIrO_3$ structure and the high-pressure-temperature phase diagram of alumina

Jun Tsuchiya,* Taku Tsuchiya,† and Renata M. Wentzcovitch
Department of Chemical Engineering and Materials Science, Minnesota Supercomputing Institute for Digital Technology and Advanced Computation, Virtual Laboratory for Earth and Planetary Materials, University of Minnesota, 421 Washington Ave. S.E., Minneapolis, Minnesota 55455, USA

(Received 21 April 2005; published 14 July 2005)

The high-pressure behavior of alumina has been investigated by first-principles computations throughout the range of calibration of the ruby pressure scale. It is found that at 0 K the transformation from corundum to Rh_2O_3(II)-type alumina at 87–113 GPa is followed by a second one to the $CaIrO_3$ structure at 150–172 GPa. Quasiharmonic free-energy calculations show that both transformations display negative Clapeyron slope, which is a consequence of the decrease in polyhedral connectivity along the structural sequence. Like the first transformation, the second one should also have significant effects on the ruby pressure scale, especially if ruby is cycled across the phase boundaries.

DOI: 10.1103/PhysRevB.72.020103 PACS number(s): 64.30.+t

Alumina is a model ceramic material with important applications in high-pressure science. It serves as window material in dynamic shock-wave experiments and when doped with chromium, makes ruby, a mineral whose fluorescence lines' frequencies are useful as pressure calibrant in diamond-anvil-cell experiments.[1–4] Alumina is also an important mineral component in earth's mantle. In the lower mantle, it appears to be incorporated almost entirely in $MgSiO_3$ perovskite, the major earth-forming phase with insignificant amounts of free alumina expected to exist.

The structural behavior of alumina under pressure has been a matter of great concern for it can affect, directly or indirectly, the frequency pressure relation of the ruby pressure scale. One major phase transformation from corundum to the Rh_2O_3(II) structure was theoretically predicted[5–7] and experimentally confirmed to take place at ~100 GPa in combined high-pressure, high-temperature experiments.[8,9] The phase boundary for this transformation has not been constrained yet but temperature is evidently a key factor for overcoming kinetic hindrances associated with this transformation.[8,9] This transformation should also destabilize this mineral component in $MgSiO_3$ perovskite in the lower mantle and perhaps have significant consequences for the mineralogy of the lowermost part of this region. A second transformation from the Rh_2O_3(II) structure to *Pbnm* perovskite was also predicted theoretically to occur above ~223 GPa (Ref. 7). Here we show by first-principles computations that alumina in the $MgSiO_3$ structure transforms to the $CaIrO_3$ structure at 150~170 GPa, eclipsing entirely the perovskite phase. Using quasiharmonic (QHA) free-energy calculations coupled with first-principles vibrational densities of states we also determine the phase boundaries for both transformations.

The structural sequence from corundum to *Pbnm* perovskite is reminiscent of hematite, i.e., Fe_2O_3 in the corundum structure. Hematite undergoes a phase transition at 30 GPa to what today appears to be the *Pbnm* perovskite structure,[10] even though the diffraction patterns of *Pbnm* perovskite and of Rh_2O_3(II) structures are very similar,[9] and for some time hematite was thought to transform to the Rh_2O_3(II) structure.[11,12] $MgSiO_3$ also has a similar structural sequence from corundum-type ilmenite to *Pbnm* perovskite, the major earth-forming phase. Recently, a new polymorph with the $CaIrO_3$-type structure (*Cmcm* symmetry) has been shown experimentally and theoretically to occur after *Pbnm* perovskite in $MgSiO_3$ at pressure and temperature (P,T) conditions similar to those expected near the core mantle boundary (~120 GPa and ~2500 K) (Refs. 13–16). This postperovskite transition has recently been reported or predicted in other compounds[17,18] including Fe_2O_3 with a transition pressure of 50 GPa (Refs. 10 and 19).

Our computations have been performed within the local-density approximation (LDA) (Refs. 20 and 21) and the generalized gradient approximation (GGA) (Ref. 22). The Troullier-Martins pseudopotentials[23] for Mg, Si, O, and Al have already been extensively tested.[14,24–26] The plane-wave cutoff was chosen as 70 Ry and the Brillouin zone was sampled on $4\times4\times4$ (10 points), $4\times4\times4$ (4 points), $4\times4\times2$ (4 points), and $4\times4\times2$ (6 points) Monkhorst-Pack mesh[27] for corundum, Rh_2O_3(II), *Pbnm* perovskite, and *Cmcm* $CaIrO_3$ structures, respectively. Structures were optimized using damped variable-cell-shape molecular dynamics.[28] The effects of using larger cutoff and k points on the calculated properties are found to be insignificant. Phonon calculations were performed using density-functional perturbation theory (DFPT) (Ref. 29). The Brillouin-zone sampling for phonon states was computed on 6, 8, 8, and 6 q points for corundum, Rh_2O_3(II), perovskite, and $CaIrO_3$ structures, referred to as postperovskite from now on, respectively.

The four crystal structures relevant to alumina, hematite, and $MgSiO_3$ are shown in Fig. 1. They can be grouped in two pairs of distinct types: (a) corundumlike and Rh_2O_3(II) structurelike, and (b) perovskite and postperovskite. Type (a) structures are energetically favored at low pressures. Their cation polyhedra are all of the same type, octahedra, and have similar sizes. Type (b) structures are energetically favored at higher pressures. These structures have two distinct

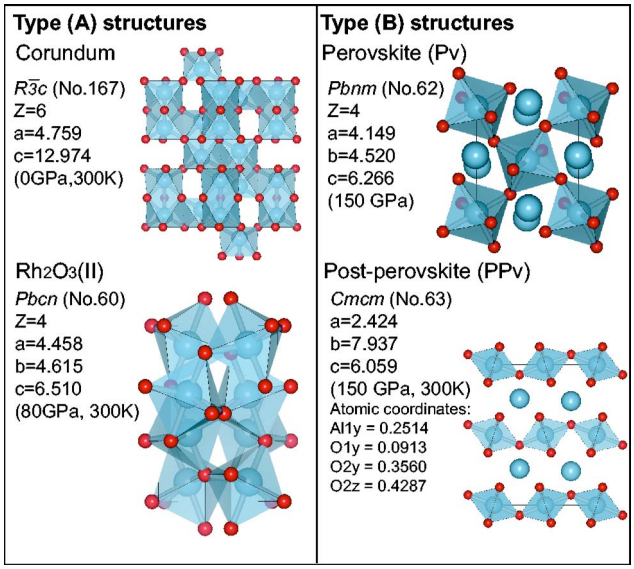

FIG. 1. (Color online) Four crystal structures of alumina. Large spheres, octahedra, and small spheres are Al, AlO_6, and O, respectively.

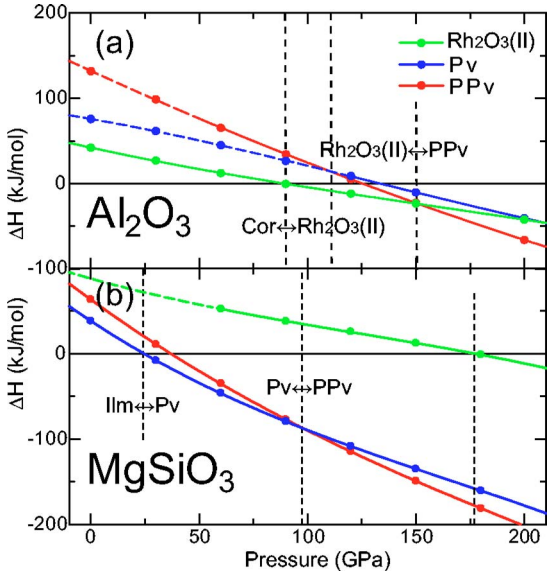

FIG. 2. (Color online) Relative enthalpy of (a) Al_2O_3 and (b) $MgSiO_3$ polymorphs with respect to corundum and ilmenite.

cation polyhedral types, octahedra for the smaller cations and eightfold-coordinated polyhedra for the larger ones. The degree of polyhedral connectivity is larger in type (a) structures than in type (b): in corundum the octahedra share faces, in Rh_2O_3(II) type, the octahedra share edges, in perovskite the octahedra share only corners, and in postperovskite the octahedral network is no longer connected. It breaks into octahedral planes. Type (b) structures are therefore less rigid and more adaptable to pressure. They compress not only through bond length reduction and polyhedral distortions but also through more extensive octahedral rotations. The postperovskite structure's compression mechanism is actually very anisotropic.[25]

Figure 2 shows the relative enthalpies of Al_2O_3 and $MgSiO_3$ in these structures. The energetic relations between structural types (a) and (b) are quite striking. At low pressures alumina stabilizes simultaneously both structures of type (a) with respect to type (b). The latter stabilizes at considerably higher pressures. In contrast, in $MgSiO_3$, type (b) structures are more stable almost throughout the entire pressure range. This happens because type (a) structures favor similar cations and type (b) favor dissimilar ones by virtue of their polyhedral types. Corundum-type $MgSiO_3$, i.e., ilmenite, is still energetically favored with respect to type (b) structures in a small pressure range at low pressures but the Rh_2O_3(II) structure does not have a stability field. It is only metastable above ~60 GPa (static LDA). Below this pressure it is unstable. The transitions to perovskite and postperovskite occur, respectively, at ~24 (Ref. 24) and ~98 GPa (Ref. 14) in static LDA calculations. In contrast, in alumina it is the perovskite phase that does not have a stability field. Besides, it is unstable below ~110 GPa. In static calculations the corundum to Rh_2O_3(II) transition takes place between 87 and 113 GPa while the latter transforms directly to postperovskite between 150 and 172 GPa, the lower and upper bounds being given by LDA and GGA exchange and correlation functionals, respectively. The static LDA and GGA values of the second transition have recently been reported to be 156 and 153 GPa, respectively.[30] Although the structural sequences with pressure are distinct in alumina and in $MgSiO_3$, in both cases the degree of polyhedral connectivity decreases along the sequences. Calculated equations of states for alumina polymorphs at 300 K are in good agreement with experiments[8,9,31] [Fig. 3(a)]. Differences between previous calculation[30] and our results are likely to have been caused by the use of different pseudopotentials. The volume reductions in the first (87 GPa) and second (150 GPa) transitions are 2.0% and 2.8%, respectively.

Analyses of polyhedral volumes lend insights into the influence of alumina on the important postperovskite transition in $MgSiO_3$ within earth's lower mantle. This transformation is of fundamental geophysical significance.[34,35] A displacement of the phase boundary by ~20 GPa can prevent this transition from happening in earth. Figure 3(b) shows that the polyhedral volumes of alumina and $MgSiO_3$ are more similar in size in the perovskite than in the postperovskite phase. This implies the coupled substitution of Mg and Si by two Als should induce less stress in the perovskite than in the

TABLE I. Thermodynamic parameters of Al_2O_3 in the corundum, Rh_2O_3(II), and postperovskite structures.

	0 GPa, 300 K Corundum	80 GPa, 300 K Rh_2O_3(II)	150 GPa, 300 K Postperovskite
B_S (GPa)	242.1	531.1	764.1
$\partial B_S/\partial P$	3.93	3.32	3.31
B_T (GPa)	240.5	530.2	762.6
$\partial B_S/\partial P$	3.94	3.33	3.31
V (cm^3/mol)	25.543	20.163	17.552
γ	1.31	1.01	1.26
α (10^{-5} K^{-1})	1.71	0.59	0.53

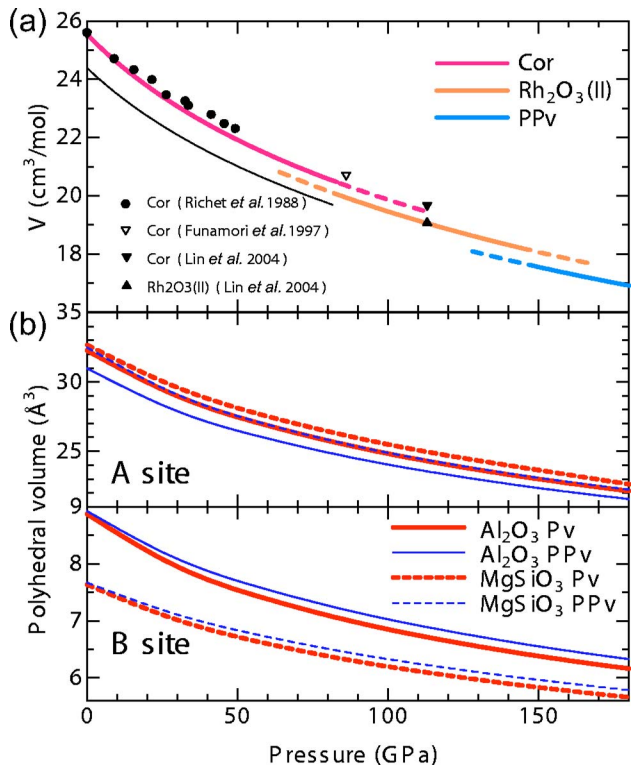

FIG. 3. (Color online) (a) Equation of states of alumina polymorphs at 300 K with experimantal results (Refs. 8, 9, and 31). The thin solid line is a static calculation (Ref. 30). (b) Polyhedral volumes of perovskite and postperovskite in Al_2O_3 and $MgSiO_3$.

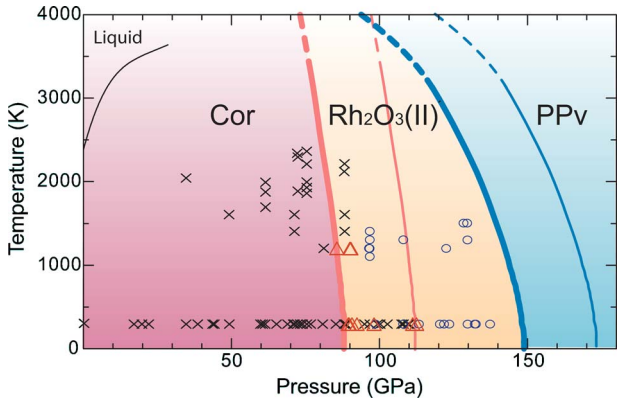

FIG. 4. (Color online) Phase boundaries for alumina polymorphs. The Clapeyron slopes from corundum to Rh_2O_3(II) and from Rh_2O_3(II) to postperovskite are −3.6 and −9.4 MPa/K at 1000 K, respectively. The thick dashed lines are the region where the QHA is invalid according the thermal expansion criterion proposed in Ref. 32. The black, thin solid line is a melting curve of corundum (Ref. 33). Black crosses, blue open circles, and red open triangles are conditions in which the corundum, Rh_2O_3(II)+corundum during compression, and Rh_3O_3+corundum under decompression were observed experimantally, respectively (Ref. 9).

postperovskite phase. Therefore, alumina should destabilize less the perovskite than the postperovskite phase of $MgSiO_3$. This has two consequences: (a) Throughout the postperovskite transformation in aluminous $MgSiO_3$, aluminum should partition more favorably in the perovskite phase in the two phases region. (b) The postperovskite transition should complete at higher pressures in solid solutions containing small amounts of alumina, as already reported.[36,37] Another manifestation of this polyhedral volume effect can also be seen in Fig. 2. The postperovskite transition occurs at 98 GPa in $MgSiO_3$ while the postperovskite enthalpy crossover in alumina takes place at ~110 GPa. This implies the solid solution should have a transition pressure a little higher than 98 GPa.

The calculated phase boundaries in alumina are shown in Fig. 4. They have not been constrained experimentally yet and should be particularly important for improving our understanding of the ruby pressure scale. Both transformations have negative Clapeyron slopes ($dP/dT=\Delta S/\Delta V$), meaning the vibrational entropy increases across the phase transitions. As argued already in the case of the ilmenite to perovskite transition in $MgSiO_3$, that also has a negative Clapeyron slope, the increase in entropy along a transition like this is related to the reduction of polyhedral connectivity.[24] The vibrational density of states of less connected polyhedral networks have their centers of mass shifted to lower frequencies due to the introduction of softer polyhedral oscillation-type modes. This is one of the changes in properties, among others, that have been identified as sources of increasing entropy across phase transitions.[38] The lower average phonon frequency of the high-pressure phase also decreases zero-point motion energy across the transition. Therefore, the transition pressures at 0 K is smaller than the static values.[24]

These phase boundaries should be kept in mind when ruby is used as a pressure calibrant. (1) Alloying alumina and Cr_2O_3, chromia, which also undergoes the corundum to Rh_2O_3(II) phase transition at lower pressures,[39,40] should lower the transition pressure of ruby's first transition. (2)The optical properties of ruby change considerably across the first phase transformation, particularly the frequency of the absorption lines.[41] The fluorescence lines are much less sensitive. (3) An indirect effect is also well known: ruby cycled across the first phase transformation retains changes in the local environment of chromium, producing a redshift in the fluorescence lines corresponding to a fossilized pressure (~5 GPa when ruby is cycled to 136 GPa and laser heated).[9] The new Rh_2O_3(II) to postperovskite transition should produce no less significant additional effects. Chromium should partition preferentially into the large *A* site of postperovskite which has even lower symmetry. The presence of 3–5 % mol of chromia may affect the second transition pressure as well; however, it is unclear how at the moment, since no postperovskite transition has been found yet in chromia.

Note added. While this paper was being prepared we received a preprint from Razvan Caracas reporting static calculations of the transitions identified here.[30]

This research was supported by NSF/COMPRES 0135533, NSF/EAR 0230319, and NSF/ITR-0428774. J.T. acknowledge the Japan Society for the Promotion of Science (JSPS).

*Present address: Geodynamics Research Center, Ehime University, Japan. Electronic address: junt@sci.ehime-u.ac.jp

†Present address: Geodynamics Research Center, Ehime University, Japan.

[1] R. Forman, G. Piermarini, J. Barnett, and S. Block, Science **174**, 284 (1972).

[2] J. Xu, H.-K. Mao, and P. Bell, Science **232**, 1404 (1986).

[3] J. H. Eggert, K. A. Goettel, and I. F. Silvera, Phys. Rev. B **40**, 5724 (1989).

[4] N. Chen and I. Silvera, Rev. Sci. Instrum. **67**, 4275 (1996).

[5] H. Cynn, D. Isaak, R. Cohen, M. Nicol, and O. Anderson, Am. Mineral. **75**, 439 (1990).

[6] F. Marton and R. Cohen, Am. Mineral. **79**, 789 (1994).

[7] K. Thomson, R. Wentzcovitch, and M. Bukowinski, Science **274**, 1880 (1996).

[8] N. Funamori and R. Jeanloz, Science **278**, 1109 (1997).

[9] J.-F. Lin, O. Degtyareva, C. T. Prewitt, P. Dera, N. Sata, E. Gregoryanz, H.-K. Mao, and R. J. Hemley, Nat. Mater. **3**, 389 (2004).

[10] S. Ono, T. Kikegawa, and Y. Ohishi, J. Phys. Chem. Solids **65**, 1527 (2004).

[11] R. D. Shannon and C. T. Prewitt, J. Solid State Chem. **2**, 134 (1970).

[12] G. K. Rozenberg, L. S. Dubrovinsky, M. P. Pasternak, O. Naaman, T. Le Bihan, and R. Ahuja, Phys. Rev. B **65**, 064112 (2002).

[13] M. Murakami, K. Hirose, K. Kawamura, N. Sata, and Y. Ohishi, Science **304**, 855 (2004).

[14] T. Tsuchiya, J. Tsuchiya, K. Umemoto, and R. M. Wentzcovitch, Earth Planet. Sci. Lett. **224**, 241 (2004).

[15] A. Oganov and S. Ono, Nature (London) **430**, 445 (2004).

[16] T. Lay, D. Heinz, M. Ishii, S. Shim, J. Tsuchiya, T. Tsuchiya, R. Wentzcovitch, and D. Yuen, EOS (Wash. D.C.) **86**, 1 (2005).

[17] K. Hirose, K. Kawamura, S. Tateno, N. Sata, and Y. Ohishi, Am. Mineral. **90**, 262 (2005).

[18] J. Parise, K. Umemoto, R. Wentzcovitch, and D. Weidner, EOS Trans. Am. Geophys. Union 85(47), abstract MR23A-0188 (2004).

[19] S. Ono and Y. Ohishi (unpublished).

[20] D. M. Ceperley and B. J. Alder, Phys. Rev. Lett. **45**, 566 (1980).

[21] J. Perdew and A. Zunger, Phys. Rev. B **23**, 5048 (1981).

[22] J. P. Perdew, K. Burke, and M. Ernzerhof, Phys. Rev. Lett. **77**, 3865 (1996).

[23] N. Troullier and J. L. Martins, Phys. Rev. B **43**, 1993 (1991).

[24] R. Wentzcovitch, L. Stixrude, B. Karki, and B. Kiefer, Geophys. Res. Lett. **31**, L10611 (2004).

[25] T. Tsuchiya, J. Tsuchiya, K. Umemoto, and R. M. Wentzcovitch, Geophys. Res. Lett. **31**, GL020278 (2004).

[26] Core cutoff radii of Al are $r_s=r_p=r_d=2.00$ a.u. (p locality).

[27] H. Monkhorst and J. Pack, Phys. Rev. B **13**, 5188 (1976).

[28] R. M. Wentzcovitch, Phys. Rev. B **44**, 2358 (1991).

[29] S. Baroni, S. de Gironcoli, A. D. Corso, and P. Giannozzi, Rev. Mod. Phys. **73**, 515 (2001).

[30] R. Caracas and R. Cohen, Geophys. Res. Lett. **32**, GL022204 (2005).

[31] P. Richet, J.-A. Xu, and H.-K. Mao, Phys. Chem. Miner. **16**, 207 (1988).

[32] R. M. Wentzcovitch, B. B. Karki, M. Cococcioni, and S. de Gironcoli, Phys. Rev. Lett. **92**, 018501 (2004).

[33] G. Shen and P. Lazor, J. Geophys. Res. **100**, 17699 (1995).

[34] A. Navrotsky, M. Schoenitz, H. Kojitani, H. Xu, J. Zhang, D. Weidner, and R. Jeanloz, J. Geophys. Res. **108**, 2330 (2003).

[35] J. Brodholt, Nature (London) **407**, 620 (2000).

[36] S. Akber-Knutson and G. Steinle-Neumann, EOS Trans. Am. Geophys. Union 85(47), abstract MR22A-08 (2004).

[37] B. Kiefer and L. Stixrude, EOS Trans. Am. Geophys. Union 85(47), abstract MR23A-0195 (2004).

[38] A. Navrotsky, Geophys. Res. Lett. **7**, 709 (1980).

[39] S.-H. Shim, T. S. Duffy, R. Jeanloz, C.-S. Yoo, and V. Iota, Phys. Rev. B **69**, 144107 (2004). This transformation in chromia occurs through an intermediate V_2O_3-type structure.

[40] A. Y. Dobin, W. Duan, and R. M. Wentzcovitch, Phys. Rev. B **62**, 11997 (2000).

[41] W. Duan, G. Paiva, R. M. Wentzcovitch, and A. Fazzio, Phys. Rev. Lett. **81**, 3267 (1998).